Journal of Power Sources 196 (2011) 8147–8153

Contents lists available at ScienceDirect

Journal of Power Sources

journal homepage: www.elsevier.com/locate/jpowsour

The role of mechanically induced separator creep in lithium-ion battery capacity fade

Christina Peabody, Craig B. Arnold*

Department of Mechanical and Aerospace Engineering Princeton University, Princeton, NJ 08544, USA

ARTICLE INFO

Article history:
Received 21 March 2011
Received in revised form 5 May 2011
Accepted 12 May 2011
Available online 19 May 2011

Keywords:
Lithium-ion battery
Power fade
Capacity fade
Mechanical stress
Aging
Polymer separator

ABSTRACT

Lithium-ion batteries are well-known to be plagued by a gradual loss of capacity and power which occur regardless of use and can be limiting factors in the development of emerging energy technologies. Here we show that separator deformation in response to mechanical stimuli that arise under normal operation and storage conditions, such as external stresses on the battery stack or electrode expansion associated with lithium insertion/deinsertion, leads to increased internal resistance and significant capacity fade. We find this mechanically induced capacity fade to be a result of viscoelastic creep in the electrochemically inactive separator which reduces ion transport via a pore closure mechanism. By applying compressive stress on the battery structure we are able to accelerate aging studies and identify this unexpected, but important and fundamental link between mechanical properties and electrochemical performance. Furthermore, by making simple modifications to the electrode structure or separator properties, these effects can be mitigated, providing a pathway for improved battery performance.

1. Introduction

Lithium-ion batteries (LIBs) are highly versatile energy storage devices for a variety of applications from large-scale electric vehicles to small-scale portable electronics [1–3]. Increases in internal resistance associated with decreased lithium-ion or electronic transport over repeated cycling has been shown to be a good indicator of capacity fade [4–11], with the majority of studies suggesting chemical modification or structural fatiguing of the electrodes during cycling as possible mechanisms [12–15]. While these studies acknowledge the fact that mechanical stresses can cause degradation of the electroactive materials, they do not address possible effects of mechanical stresses on nonelectroactive materials. Mechanical stresses on rechargeable LIBs arise from a number of sources during standard usage or storage. In certain applications, external stress is intentionally applied, such as in flexible energy storage devices or high power battery systems [16–19]. However, more commonly, stress can develop as a consequence of the internal strain during charge and discharge [15,20–24].

In this work we show how mechanical stresses can affect the electrochemical performance of LIBs through modifications to the non-electroactive polymer separator. Through a combination of mechanical and electrochemical testing of pouch type LIBs and battery components we are able to identify polymer creep induced pore closure as a deformation mechanism in the separator. First we measure the strain response of the separators under static compressive loads of varying magnitude. The separators are then physically characterized using SEM imaging and pore volume measurement techniques. The electrochemical performance of the stressed separators is characterized through electrochemical impedance spectroscopy and galvanostatic charge/discharge techniques. Finally, we discuss potential pathways for mitigating stress effects on battery polymer separators.

2. Background

2.1. Analysis of strains generated in lithium-ion battery separators due to electrode expansion

Although slight variations might exist among manufacturers, the basic structure for commercial cells consists of compressed, ceramic powder/graphite/polymer binder, electrodes on metal current collector foils and a polymer separator rolled together as shown in Fig. 1, then packaged in a polymer pouch or rigid metal canister [19]. Upon charging and discharging, lithium ions are intercalated and deintercalated into the electrode materials causing significant strain, depending on the electrode composition [20–27]. Standard polymer separators are composed of polyethylene and polypropylene layers with a yield strength of approximately 10–40 MPa, which is significantly lower than the yield strength of the metal current collectors or the ceramic electrode materials. Although there is polymer binder in the electrodes,

* Corresponding author. Tel.: +1 609 258 0250; fax: +1 609 258 5877.
E-mail address: cbarnold@princeton.edu (C.B. Arnold).

0378-7753/$ – see front matter © 2011 Elsevier B.V. All rights reserved.
doi:10.1016/j.jpowsour.2011.05.023

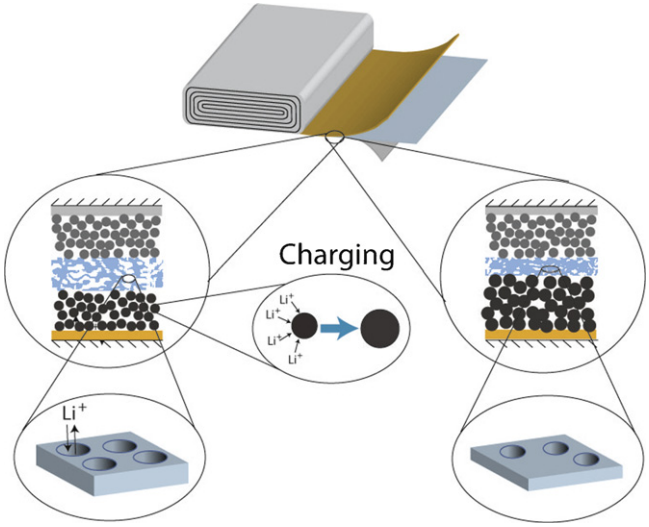

Fig. 1. Schematic of separator pore closure due to electrode expansion. Many commercial lithium-ion batteries are fabricated by winding the electrodes and separator in a jellyroll configuration. The jellyroll structure is then tightly packed into a metal canister or foil pouch. This establishes a stack pressure on the battery assembly and ensures adhesion between the electrode materials and current collectors. When the battery is charged and discharged, lithium ions intercalate and deintercalate into and out of the electrode materials leading to expansion and contraction. The constraint imposed on electrode expansion by the metal current collectors and canister result in a compressive stress and strain accommodation by the polymer separator. Our studies indicate that compressive stresses cause pore closure in the polymer separator which impedes ion transport and degrades battery performance.

these composite electrodes are prestressed with high pressures during the calendaring process [28,29], and so we expect little additional electrode deformation in response to intercalation with the separator bearing the majority of the mechanical deformation.

The amount of induced separator strain as a result of intercalation-induced expansion of the electrodes can be calculated from the electrode strain data in the literature. Consider a battery with the $LiCoO_2$/graphite electrode couple in a metal canister. The metal canister does not allow for volumetric expansion of the battery assembly during charging or discharging. For these materials it has been shown that the $LiCoO_2$ electrode linearly expands 1.6% and the graphite linearly expands 10% at full charge [25]. The thickness of the active material coating varies depending on the volumetric capacity of the cell with higher capacity cells requiring thicker electrodes, however the average electrode thickness is approximately 100 μm [30]. Lithium-ion batteries are assembled in the fully discharged state, so the electrode thickness listed above is that for a discharged battery [19].

Mechanical strain, ε, is related to the material thickness through the following equation:

$$\varepsilon = \frac{l - l_0}{l_0} \quad (1)$$

In this equation, l_0 is the electrode thickness in the fully discharged state and l is the electrode thickness in the fully charged state. So in the fully charged state, the total cathode and anode expansion in our system would be 11.6 μm. Most battery separators are at most 40 μm thick, however more typically the separators are 20–25 μm in thickness. Therefore, the amount of strain that would be induced in the separator as a result of the electrode strain could be as high as 25–50%.

2.2. External sources of stress in battery systems

While electrochemically induced effects may lead to separator strain, direct application of stresses to the battery stack may also occur which would induce viscoelastic creep in the separator as a result of stress accommodation. Such stresses can arise under normal operation, for instance batteries operating in high pressure environments, electric/hybrid vehicles or flexible applications. In canister type cells, an external stress known as the stack pressure is applied to the jellyroll in order to ensure intimate contact between the electrodes [19]. Pouch type lithium-ion battery electrodes are bonded so that stack pressure is not necessary to maintain electrode contact. However, since these cells are packaged in flexible aluminum-laminate foil pouches, stresses applied externally to the package are accommodated by the battery stack. One example of this would be a laptop battery in which the polymer cells are contained in a rigid case, during charging the case resists the cell's expansion, thus exerting a stress on the battery stack. Furthermore, the adaptation of this technology for thin-film flexible batteries means that the battery stack and particularly the separator could be subject to more complex bending stress conditions.

3. Experimental methods

3.1. Mechanical testing of commercial lithium-ion pouch type cells and cell components

We have mechanically tested prismatic pouch type lithium-ion batteries obtained from Powerstream Technologies, Inc. and Plantraco, Ltd. The dimensions and nominal capacities of the batteries are given in Table 1. Each battery is cycled three times at a C/2 rate using a constant-current/constant-voltage (CCCV) protocol prior to mechanical testing to ensure that the battery is not defective. The battery results reported in this work are those of the 90 mAh Powerstream batteries tested at 3.0 V.

The batteries are mechanically tested using an Instron electromechanical universal testing system. The battery strain is measured with a linear variable differential transformer (LVDT) mounted to the Instron crosshead. An Arbin MSTAT potentiostat is used to measure the open circuit voltage of the battery during the tests to ensure that the applied stress does not cause internal shorting. The battery is initially placed under a compressive stress of 1 MPa for 5 min in order to compress the excess volume in the pouch. The load is then removed for 5 min to allow for relaxation and elastic recovery in the cell. The cell is then loaded to a static stress of 1–30 MPa for 3 h. For both the preload and load steps the stress is applied uniaxially to the large prismatic face of the battery. After mechanical testing the batteries are cycled electrochemically according to the protocol outlined above, again to ensure that mechanical testing has not shorted the battery.

Samples of polymer separator are also tested, as well as samples of polymer separator sandwiched between foil current collectors. For the polymer separator tests, Celgard® 2340 separator is wound

Table 1
Dimensional parameters and nominal capacities of commercial cells and SF systems.

Sample	Nominal capacity (mAh)	Length (cm)	Width (cm)	Thickness (mm)
Battery A	90	1.759 ± 0.004	1.095 ± 0.004	4.192 ± 0.055
Battery B	160	2.408 ± 0.038	1.269 ± 0.004	4.874 ± 0.084
SF Jellyroll	N/A	2.073 ± 0.029	1.827 ± 0.100	2.845 ± 0.347
SF Plates	N/A	2.095 ± 0.457	1.538 ± 0.083	2.204 ± 0.099

into a jellyroll similar to the electrode-separator laminate in prismatic batteries; for the separator and foil (SF) tests, the polymer separator is sandwiched between aluminum and copper foil sheets then wound in a jellyroll configuration. The SF samples are wound so that the aluminum foil is the outer layer and the copper foil is the inner layer. Table 1 shows the geometry of the separator and SF samples that are mechanically tested as described above for the batteries.

The effect of non-uniform stresses on the separator materials is characterized by placing a perforated stainless steel plate between the bottom platen of the Instron and the jellyrolled separator sample. The perforated steel plate has evenly spaced holes 4.75 mm in diameter that results in 40% open area. The static force applied to the separator corresponds to 30 MPa for a uniformly applied load. The mechanical load testing procedure is the same as previously outlined.

3.2. Physical and electrochemical characterization of stressed Celgard® separators

Physical and electrochemical analyses are performed on the stressed, jellyrolled Celgard® 2340 separators. The microstructure of the separators is characterized using a Philips FEG scanning electron microscope. 1.27 cm diameter circles are cut from the mechanically stressed separators for imaging. The samples are coated with 3 nm of iridium to enhance the surface conductivity for clearer imaging. The images are taken at 50,000× magnification with an accelerating voltage of 15 kV and a spot size of 3.0.

The pore volume of the separators is measured by comparing the density of the separator to the density of the bulk separator polymer. The density of the bulk polymer is 0.91 g cm^{-3} as reported in the literature [31]. The density of the stressed separators is obtained by measuring the thickness and mass of 1.27 cm diameter discs.

The ionic conductivity of polymer separator samples is measured using electrochemical impedance spectroscopy. The compressed polymer samples are cut into 1.27 cm diameter discs which are soaked in liquid lithium-ion electrolyte composed of $LiPF_6$ salt in a 1:1 EC/DEC solution. The separator discs are then placed between two stainless steel electrodes in a Swagelok® t-cell. Electrochemical impedance measurements are made using a Solartron 1260 FRA coupled with a Solartron 1287 electrochemical interface. The frequency of the voltage input is swept between 60 kHz and 100 mHz, with a mean voltage of 0 V and an amplitude of 10 mV. Samples of the unstressed polymer separator are tested according to the same protocol.

Finally, the effect of the mechanical stress on the separator performance during electrochemical cycling is measured in a Swagelok® t-cell. A 1.27 cm diameter disc is cut from the cathode of a commercial battery. The active material is scraped off one side of the disc to ensure good electrical contact between the stainless steel plug and the aluminum current collector on the electrode. The cathode disc is cycled vs. Li foil with the same electrolyte composition used in the ionic conductivity tests described above. The cell is cycled 5 times with charge and discharge currents of 0.5 mA. The cell is then disassembled and while the same electrodes are used, the unstressed separator is replaced with a stressed separator and the electrolyte replenished. The cell is then cycled again with the same charge and discharge currents. In order to ensure that any measured capacity loss is not due to the cathode the cell is cycled again with an unstressed separator.

4. Results and discussion

In order to understand and characterize the relationship between mechanical properties of non-electroactive components and the battery's electrochemical performance, we apply external compressive stresses of different magnitude and analyze the strain response of the composite structure. By applying stresses as high as 30 MPa, we can accelerate longer term creep studies allowing quantitative data to be acquired in a significantly reduced time frame. Fig. 2(a) shows the temporal strain response of a pouch type lithium-ion battery to a static compressive stress of 30 MPa. The battery exhibits an initial rapid increase in compressive strain followed by a gradual increase in strain over time. This response is characteristic of viscoelastic creep, a common deformation mechanism for polymeric materials experiencing static loads. In our batteries, there are three main polymer sources, the external packaging, the electrode binder and the separator. The thickness of the packaging is small compared to the overall battery thickness and so its contribution to the total deformation is minimal. In addition, the polymer binder has previously been subjected to comparable or higher stresses during the calendaring process than those used in our test [28,29] and so one would not expect any

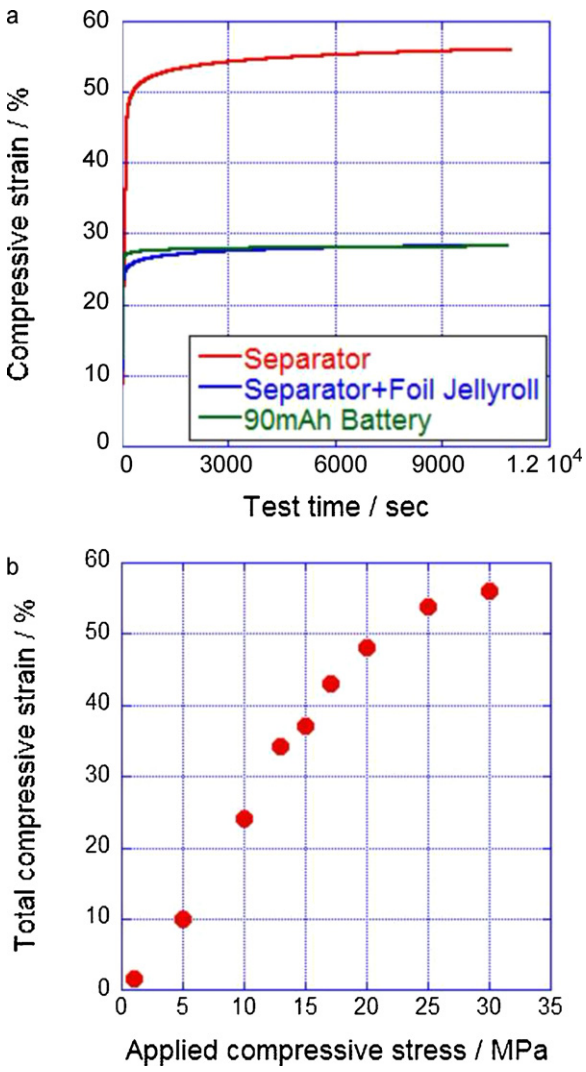

Fig. 2. Stress strain data for lithium-ion battery materials. (a) Comparison of the temporal strain response of a 90 mAh pouch type lithium-ion battery with that of a separator jellyroll and a separator/current collector foil jellyroll under a 30 MPa applied stress at room temperature. The separator material exhibits a much larger strain than the battery and the SF samples because of its low yield stress. (b) The total plastic strain in the separator jellyroll as a function of applied stress after 3 h. Linear behavior is expected from viscoelastic modeling while the divergence from linearity at high stress is due to the onset of a different deformation mechanism in the polymer separator.

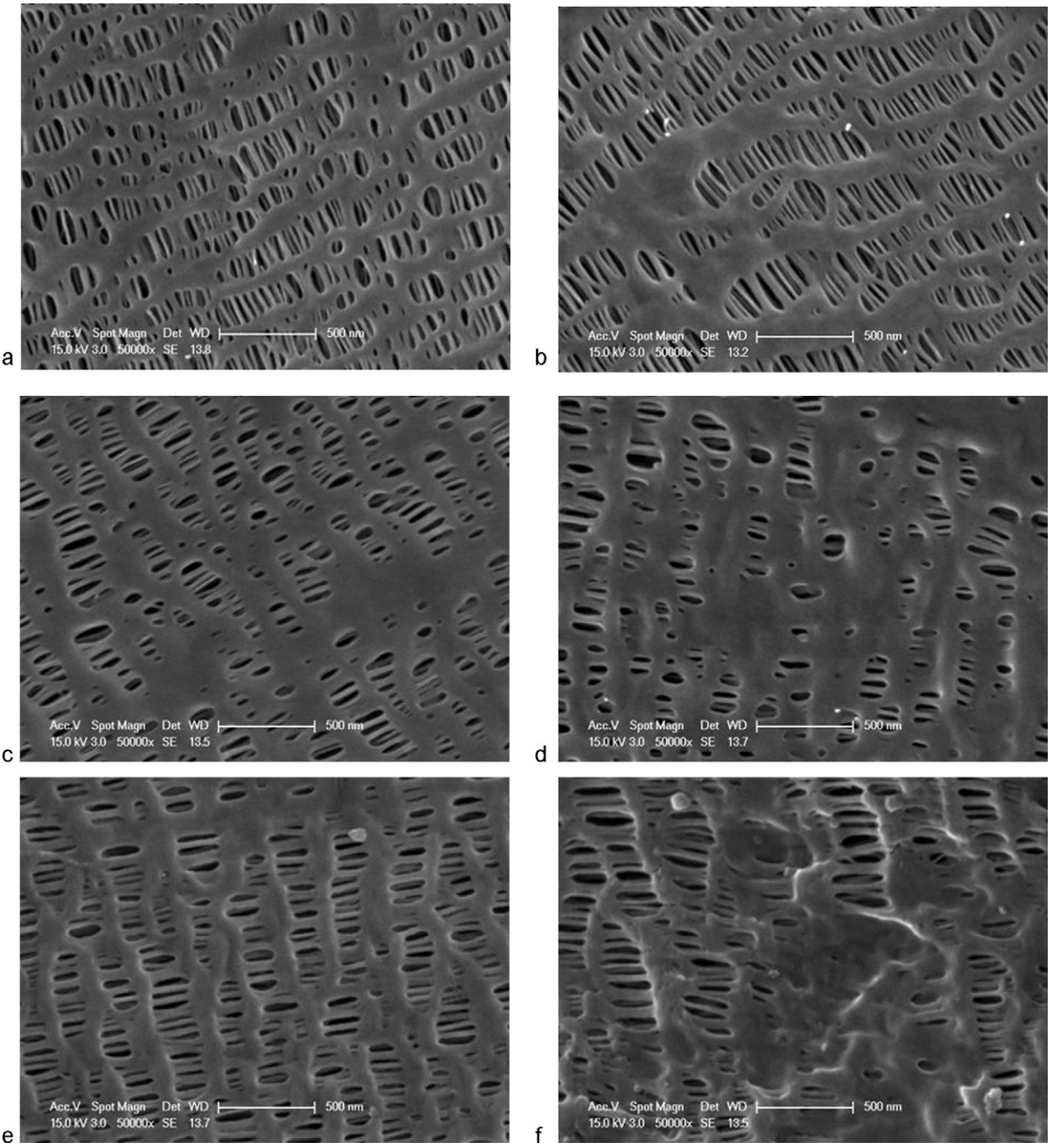

Fig. 3. Images of viscoelastic creep induced pore closure. SEM characterization of separator membranes after compressive stress testing. (a) Unstressed, (b) 5 MPa, (c) 10 MPa, (d) 30 MPa from separator only tests. Increasing total strain associated with higher stress decreases the pore areal density. (e) Unstressed separator from 90 mAh battery, (f) separator from a 90 mAh battery stressed at 30 MPa. The presence of electrolyte does not prevent stress-induced pore closure. The scale bar represents 500 nm for all of the images.

further significant deformation to occur. Therefore, we attribute the measured creep deformation to the polymer separator which is supported by the data in Fig. 2(a). Here, rolled samples of the polypropylene/polyethylene separator alone and with metal foil current collectors are tested, revealing that as expected from the relative strengths of materials, a spatially confined separator can account for the total deformation and serve as a simplified model system to understand the overall effects of stress on the entire battery.

As far as the separator is concerned, external stress is equivalent to stress induced by electrode strain. Upon volumetric expansion, electrodes will exert a stress on both the separator and the current collectors/packaging. However, since the polymer separator has a lower yield strength, this strain will be accommodated through separator deformation and similar viscoelastic creep as in the case of externally applied forces. Under these creep conditions, the total compressive strain on the separator will depend on temperature, stress and time, with increases in temperature or stress leading to shorter times for equivalent deformation. Standard models, such as the mechanical systems based Burgers model or the empirically derived Findlay–Khosla–Peterson (FKP) model, describe these dependences [32] and enable us to extract viscoelastic parameters from separator creep strain data over short time periods, such as our 3 h tests. With the experimentally defined parameters for either

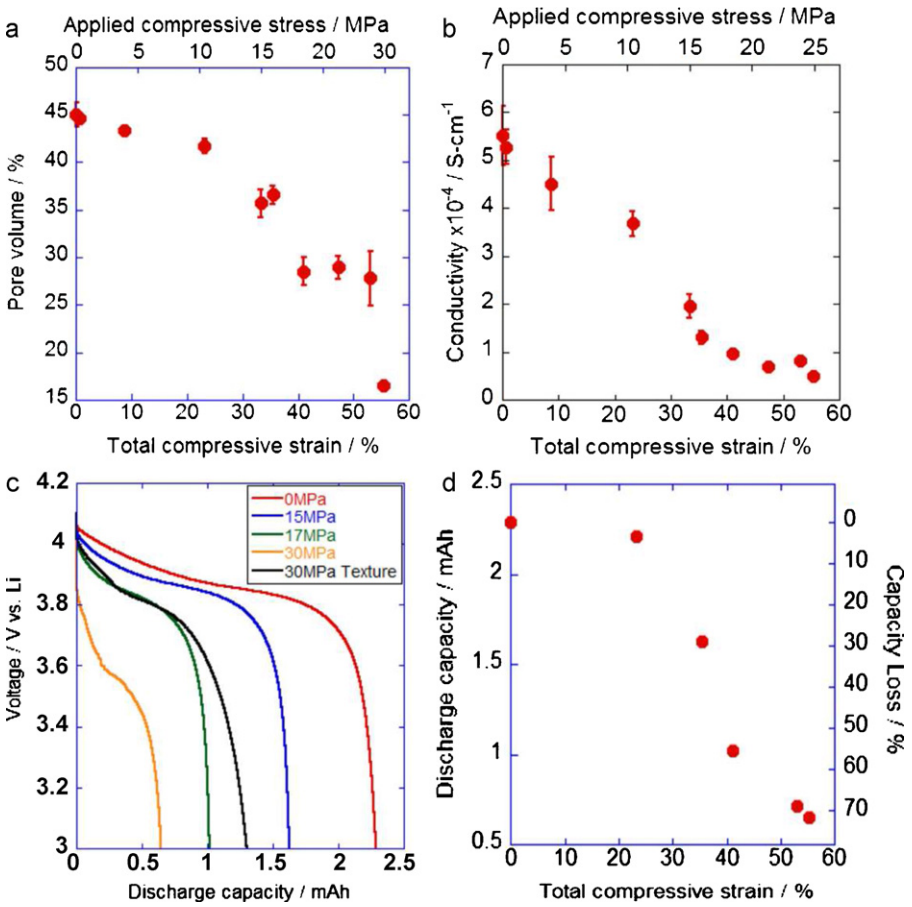

Fig. 4. Electrochemical effects of separator pore closure. (a) Pore volume of separators as a function of total strain on lower axis and applied stress on upper axis. Pore volume is measured by comparing the density of the separator membrane with that of the polymer material (0.91 g cm^{-3}). (b) Separator conductivity vs. total strain. Conductivity is measured by impedance spectroscopy. (c) Discharge curves of a $LiCoO_2$ vs. Li metal cell with $LiPF_6$ in a1:1 EC:DEC electrolyte showing the effect of stress on the separator. Notice that when the stress is applied to the separator through a textured plate the discharge capacity is greatly improved. The discharge capacity as a function of total strain is extracted from these discharge curves and summarized in part (d). For the capacity measurements, the same electrodes are used, only the separator is changed and the electrolyte replenished, thereby isolating the effects of electrochemical electrode modification and separator creep.

of the models, it is then possible to predict the strain response at longer times using the time dependent strain equation defined by the particular model [33]. Based on this understanding and assuming the creep mechanism does not change with stress, one can view mechanical testing at higher external stress as a means of accelerated testing for the lower stresses that occur due to internal strain under normal operation.

The total creep strain that occurs in a given material under static loading is dependent on the amount of time for which the load is applied and the magnitude of the applied load. Fig. 2(b) shows the strain response of the separator material for different stress values after 3 h, and as expected, larger stresses significantly increase the amount of creep strain that occurs in a given period of time. The linear relationship between stress and total strain is consistent with models for viscoelastic creep [32,33], while the deviation from linearity at high stress is due to a change in the deformation mechanism responsible for pore closure. Although the time scale of this experiment is fairly short relative to typical battery lifetimes (2–3 years), we notice significant creep of the separator at stresses as low as 5 and even 1 MPa, which is on the order of typical stack pressures found in high power LIBs. To further put this into perspective, the average pinch strength (the force generated by pinching the thumb and index finger together) exerted by an adult male corresponds to a stress of 0.8 MPa [34].

We determine the effect of viscoelastic creep of the separator on overall cell degradation by characterizing the microstructure and electrochemical properties after mechanical testing. As described schematically in Fig. 1, we hypothesize that the primary separator strain and deformation mechanism is polymer creep into the pores, leading to closure which limits the ability of lithium ions to move across the barrier. The SEM images in Fig. 3 confirm this hypothesis. As the images demonstrate, the pore density decreases with increasing stress or equivalently, total strain, in the 3 h mechanical tests. The unstressed separator and the 1 MPa separator have similar structures characterized by a large number of slit-like pores on the order of 100 nm in the long dimension and 30–40 nm in the short direction. As the applied stress increases, there is a noticeable decrease in the number of pores as smaller pores close and larger pores shrink. Finally the 30 MPa separator has a pore area fraction half that of the unstressed sample. In the case of a complete battery shown in Fig. 3 we see a similar response between the unstressed separator (Fig. 3(e)) and the 30 MPa separator (Fig. 3(f)), further verifying the separator only studies and demonstrating that the presence of electrolyte in the cell does not prevent stress-induced pore closure. The SEM results are further quantified through the pore volume measurements shown in Fig. 4(a) as plotted vs. the total strain. While the unstressed separator has a pore volume of 45%, the pore volume decreases non-linearly with increasing strain. Notice that for an applied stress of 30 MPa, the pore volume decreases to almost one third of the original unstressed value.

This decrease in pore volume impedes ion transport and manifests itself as an increase in the internal resistance of the membrane,

or conversely as a decrease in conductivity. Fig. 4(b) shows that compressive strains as low as 2% cause a measurable decrease in conductivity and that for strains above 40%, ionic conductivity is drastically decreased by a factor of 2 as compared to the unstressed membrane. In terms of applied stress the strains measured in our experiments correspond to measurable decreases in conductivity at stresses as low as 1 MPa for 3 h while stresses above 15 MPa cause significant decreases in conductivity.

To further relate the decreases in pore volume and conductivity to battery capacity, Fig. 4(c) compares the discharge curves for cells composed of unstressed electrodes with stressed separators. While stressed separators maintain the characteristic cell discharge shape, there is a marked capacity fade and reduction in discharge time as the stress increases. Fig. 4(d) represents this more clearly by extracting the capacity as a function of strain based on the discharge curves in Fig. 4(c). The cell capacity decreases with increasing stress and corresponding total separator strain, with the 30 MPa sample losing more than 70% of its capacity due to the transport limitations. The observed capacity losses occur as pore closure decreases the number and size of pathways for ions to shuttle between the electrodes during charging and discharging. This limits the ability of ions to reach reaction sites at a given charge/discharge rate and thus limits the amount of energy that is stored/used [35].

Fig. 4 demonstrates that mechanical deformation of the non-electroactive separator can cause an apparent decrease in cell capacity by limiting ionic transport and increasing the internal resistance of the cell. There remain many proposed mechanisms for LIB capacity fade in the literature and our results can occur in combination, either dominating, or amplifying these other processes. For instance, previous studies on aging of lithium-ion batteries that focused on the electrochemically active electrode materials, have shown that internal resistance can increase as a result of numerous chemical and mechanical degradation mechanisms [5–9,13]. These studies have shown increases in the film resistance of the solid electrolyte interface (SEI) as a result of unavoidable side reactions in the cell [6,8,9,13]. Additionally, mechanical fracture of electrode particles as a result of intercalation induced fatigue has been shown to increase the electrode resistance and decrease the overall cell capacity [15,20,21]. The relative importance of the different degradation mechanisms is still a topic of debate and our results bring an important new dimension of understanding to this discussion.

Based on our mechanical interpretation of capacity fade due to accumulated separator strain caused by internal or external stress, one can suggest a number of approaches to overcome this form of performance degradation. For instance, the development of separator materials with higher yield strengths would allow the battery system to accommodate higher stresses with a correspondingly lower creep strain rate. But even using existing polymeric separator materials, it is possible to mitigate the effects of electrode strain and external stress by structuring the electrodes in order to localize the strain. We simulate this concept by applying a compressive stress to the separator through a perforated metal sheet with 40% open area. In this case, we apply the same force as in the 30 MPa sample and the average creep strain reaches the same level as given in Fig. 2. As shown in Fig. 4(c), the capacity of the cell is a factor of 2 higher when texturing is employed as compared to the traditional sample. This result suggests using textured electrodes can significantly decrease the capacity fade and increase the cycle life of an LIB. Furthermore, it opens the door to additional optimization and structure design leading to further improvements in performance.

5. Conclusions

Although it is commonly believed that the causes of capacity fade and decreased power output in lithium-ion batteries are primarily chemical in nature, we show that purely mechanical mechanisms can play a significant role in this aging behavior. We demonstrate that viscoelastic creep of porous separators in lithium-ion batteries reduces ion transport via pore closure, resulting in increased internal resistance and significant capacity fade. Such effects can occur whether the battery is actively being charged or being stored in a charged state and have general applicability beyond the specific system studied here to other battery chemistries and structures in which external stress or internal strain plays a role in normal operating conditions. We find that even small external stresses as low as 1 MPa can have a measurable effect on the capacity of the system, especially when accumulated over the cell operating lifetime. By applying static external stress at elevated levels, we are able to effectively simulate long time viscoelastic creep behavior in shorter time experiments, allowing us to identify an important link between the mechanical properties of electrochemically inactive separators and the overall electrochemical performance of the system. Elevated temperature will additionally increase the creep rate, further amplifying these mechanical effects. Finally, maintaining the battery chemistry, but incorporating minor changes in the separator material or structure of the electrodes can help to significantly minimize the negative mechanical response, providing new pathways for improving battery performance.

Acknowledgements

Support for this research was provided by the Office of Naval Research and Princeton University. C.P. acknowledges support from the National Science Foundation (NSF) Graduate Research Fellowship Program. We acknowledge the usage of the PRISM Imaging and Analysis Center, which is supported in part by NSF-MRSEC.

References

[1] J.M. Tarascon, M. Armand, Nature 414 (2001) 359–367.
[2] K. Kang, Y. Meng, J. Breger, C. Grey, G. Ceder, Science 311 (2006) 977–980.
[3] D. Lindley, Nature 463 (2010) 7277.
[4] D. Zhang, B. Haran, A. Durairajan, R.E. White, Y. Podrazhansky, B.N. Popov, J. Power Sources 91 (2000) 122–129.
[5] G. Ning, B. Haran, B. Popov, J. Power Sources 117 (2003) 160–169.
[6] M. Broussely, S. Herreyre, P. Biensan, P. Kaztejna, K. Nechev, R. Staniewicz, J. Power Sources 97–98 (2001) 13–21.
[7] J. Shim, R. Kostecki, T. Richardson, X. Song, K.A. Striebel, J. Power Sources 112 (2002) 222–230.
[8] J. Vetter, P. Novak, M. Wagner, C. Veit, K.C. Moller, J. Besenhard, M. Winter, M. Wohlfahrt-Mehrens, C. Vogler, A. Hammouche, J. Power Sources 147 (2005) 269–281.
[9] K. Amine, C. Chen, J. Liu, M. Hammond, A. Jansen, D. Dees, I. Bloom, D. Vissers, G.L. Henriksen, J. Power Sources 97-98 (2001) 684–687.
[10] A.P. Schmidt, M. Bitzer, A.W. Imre, L. Guzzella, J. Power Sources 195 (2010) 7634–7638.
[11] J. Li, E. Murphy, J. Winnick, P. Kohl, J. Power Sources 102 (2001) 294–301.
[12] R. Jungst, G. Nagasubramanian, H. Case, B. Liaw, A. Urbina, T. Paez, D. Doughty, J. Power Sources 119-121 (2003) 870–873.
[13] M. Dubarry, V. Svoboda, R. Hwu, B. Liaw, J. Power Sources 165 (2007) 566–572.
[14] G. Amatucci, J. Tarascon, J. Electrochem. Soc. 149 (2002).
[15] H. Wang, Y. Jang, B. Huang, D. Sadoway, Y. Chiang, J. Electrochem. Soc. 146 (2) (1999).
[16] L. Hu, H. Wu, F. La Mantia, Y. Yang, Y. Cui, ACS Nano 4 (2010) 5843–5848.
[17] T. Pereira, R. Scaffaro, S. Nieh, J. Arias, Z. Guo, H.T. Hahn, J. Micromech. Microeng. 16 (2006) 2714–2721.
[18] T. Pereira, R. Scaffaro, Z. Guo, S. Nieh, J. Arias, H. Hahn, Adv. Eng. Mater. 10 (2008) 393–399.
[19] W. van Shalkwijk, B. Scrosati, Advances in Lithium-Ion Batteries, Kluwer Academic Publishers, 2002.
[20] J. Christensen, J. Newman, J. Solid State Electrochem. 10 (2006) 293–319.
[21] X. Zhang, W. Shyy, A.M. Sastry, J. Electrochem. Soc. 154 (10) (2007) A910.
[22] S. Renganathan, G. Sikha, S. Santhanagopalan, R.E. White, J. Electrochem. Soc. 157 (2) (2010) A155.
[23] S. Pyun, J. Go, T. Jang, Electrochim. Acta 49 (2004) 4477–4486.
[24] T. Ohzuku, Y. Iwakoshi, K. Sawai, Solid State Ionics 69 (1994).
[25] Y. Koyama, T. Chin, U. Rhyner, R. Holman, S. Hall, Y.M. Chiang, Adv. Funct. Mater. 16 (2006) 492–498.
[26] J. Reimers, J. Dahn, J. Electrochem. Soc. 140 (1993).
[27] X. Xiao, W. Wu, X. Huang, J. Power Sources 195 (2010) 7649–7660.

[28] K.A. Striebel, A. Sierra, J. Shim, C.W. Wang, A.M. Sastry, J. Power Sources 134 (2004) 241–251.
[29] C.W. Wang, Y.B. Yi, A.M. Sastry, J. Shim, K.A. Striebel, J. Electrochem. Soc. 151 (9) (2004) A1489–A1498.
[30] D. Linden, Handbook of Batteries, 3rd ed., McGraw-Hill, 2002.
[31] P. Arora, Z. Zhang, Chem. Rev. 104 (2004).
[32] S. Rosen, Fundamental Principles of Polymeric Materials, 2nd ed., Wiley, 1993.
[33] W. Findley, J. Lai, K. Onaran, Creep and Relaxation of Nonlinear Viscoelastic Materials with an Introduction to Linear Viscoelasticity, 1976 (North-Holland).
[34] V. Mathiowetz, N. Kashman, G. Volland, K. Weber, M. Dowe, S. Rogers, Arch. Phys. Med. Rehabil. 66 (1985) 69–72.
[35] M. Doyle, J. Newman, A.S. Gozdz, C. Schmutz, J. Tarascon, J. Electrochem. Soc. 143 (6) (1996) 1890–1903.